Published in final edited form as:
*Neurobiol Dis*. 2014 August ; 68: 137–144. doi:10.1016/j.nbd.2014.04.011.

# Intramitochondrial $Zn^{2+}$ accumulation via the $Ca^{2+}$ uniporter contributes to acute ischemic neurodegeneration

**Yuliya V. Medvedeva**[a] and **John H. Weiss**[b]
Departments of Neurology & Anatomy and Neurobiology, University of California Irvine, Irvine, CA 92697

## Abstract

$Ca^{2+}$ and $Zn^{2+}$ have both been implicated in the induction of acute ischemic neurodegeneration. We recently examined changes in intracellular $Zn^{2+}$ and $Ca^{2+}$ in CA1 pyramidal neurons subjected to oxygen glucose deprivation (OGD), and found that $Zn^{2+}$ rises precede and contribute to the onset of terminal $Ca^{2+}$ rises ("$Ca^{2+}$ deregulation"), which are causatively linked to a lethal loss of membrane integrity. The present study seeks to examine the specific role of intramitochondrial $Zn^{2+}$ accumulation in ischemic injury, using blockers of the mitochondrial $Ca^{2+}$ uniporter (MCU), through which both $Zn^{2+}$ and $Ca^{2+}$ appear able to enter the mitochondrial matrix. In physiological extracellular $Ca^{2+}$, treatment with the MCU blocker, Ruthenium Red (RR), accelerated the $Ca^{2+}$ deregulation, most likely by disrupting mitochondrial $Ca^{2+}$ buffering and thus accelerating the lethal cytosolic $Ca^{2+}$ overload. However, when intracellular $Ca^{2+}$ overload was slowed, either by adding blockers of major $Ca^{2+}$ entry channels or by lowering the concentration of $Ca^{2+}$ in the extracellular buffer, $Ca^{2+}$ deregulation was delayed, and under these conditions either $Zn^{2+}$ chelation or MCU blockade resulted in similar further delays of the $Ca^{2+}$ deregulation. In parallel studies using the reactive oxygen species (ROS) indicator, hydroethidine, lowering $Ca^{2+}$ surprisingly accelerated OGD induced ROS generation, and in these low $Ca^{2+}$ conditions, either $Zn^{2+}$ chelation or MCU block slowed the ROS generation. These studies suggest that, during acute ischemia, $Zn^{2+}$ entry into mitochondria via the MCU induces mitochondrial dysfunction (including ROS generation) that occurs upstream of, and contributes to the terminal $Ca^{2+}$ deregulation.

### Keywords

hippocampal slice; mitochondria; zinc; calcium; ischemia; Ruthenium Red; RU360; mitochondrial $Ca^{2+}$ uniporter; reactive oxygen species; ROS



[b]**Corresponding Author:** J. H. Weiss, MD, Ph.D., Department of Neurology, University of California, Irvine, Irvine, CA 92697-4299, USA, Ph: (949) 824-6774, Fax: (949) 824-1668, jweiss@uci.edu.
[a]Y. V. Medvedeva, Ph.D., Department of Neurology, University of California, Irvine, Irvine, CA 92697-4299, USA, yvmedved@uci.edu

## Introduction

Although relatively short periods of cerebral ischemia can result in irreversible neuronal damage, the factors underlying the high ischemic vulnerability of brain tissue are incompletely understood. A contributory factor is the rapid influx of $Ca^{2+}$ ions resulting from uncontrolled release of the excitatory neurotransmitter, glutamate, leading to the occurrence of sharp $Ca^{2+}$ rises ("$Ca^{2+}$ deregulation") indicative of cell death (Randall and Thayer, 1992; Rothman and Olney, 1986; Siesjo, 1988). However, accumulating evidence supports critical contributions of another divalent cation, $Zn^{2+}$, which is present in the brain at high levels. It accumulates in hippocampal pyramidal neurons after ischemia or prolonged seizures, and has also been implicated in ischemic neurodegeneration (Calderone et al., 2004; Frederickson et al., 1989; Koh et al., 1996; Tonder et al., 1990; Yin et al., 2002). Furthermore, like $Ca^{2+}$, exogenous $Zn^{2+}$ can be sequestered by mitochondria and impair their function (Dineley et al., 2003; Shuttleworth and Weiss, 2011; Weiss et al., 2000). In addition, recent studies in hippocampal slice models have found that extracellular and intracellular $Zn^{2+}$ levels increase shortly after onset of oxygen glucose deprivation (OGD) (Carter et al., 2011; Medvedeva et al., 2009; Stork and Li, 2006; Wei et al., 2004), and other studies have provided evidence that $Zn^{2+}$ contributes to mitochondrial dysfunction following *in vivo* ischemia (Bonanni et al., 2006; Calderone et al., 2004).

We have used acute hippocampal slice models to attempt to discriminate contributions of $Zn^{2+}$ vs $Ca^{2+}$ to acute OGD-induced degeneration of CA1 pyramidal neurons. In our prior work, we found $Zn^{2+}$ rises to precede the sharp $Ca^{2+}$ rises (termed "$Ca^{2+}$ deregulations"; Figure 1A). Additionally, it was apparent that the $Ca^{2+}$ deregulation events were causatively linked to a terminal loss of membrane integrity, since loss of membrane integrity (as indicated by rapid loss of fluorescent dye from the cell) began promptly after the sharp $Ca^{2+}$ rises, and was prevented if $Ca^{2+}$ was removed from the media during OGD, occurring only after restoration of the $Ca^{2+}$ (Medvedeva et al., 2009). If $Zn^{2+}$ was chelated, the $Ca^{2+}$ deregulation (indicative of cell death) was delayed, implicating a contribution of $Zn^{2+}$ to the terminal sequence of events. Furthermore, our results suggested that the $Zn^{2+}$ entered mitochondria and affected their function, but did not clearly determine whether the $Zn^{2+}$ effects were dependent upon the mitochondrial $Zn^{2+}$ entry (Medvedeva et al., 2009).

A central aim of the present study was thus to further examine the specific mechanisms through which $Zn^{2+}$ contributes to the sequence of events during acute OGD that culminates in the terminal $Ca^{2+}$ deregulation, specifically addressing the question of the dependence of its effects upon uptake into mitochondria. Our findings support the hypothesis that early $Zn^{2+}$ entry into mitochondria through the mitochondrial $Ca^{2+}$ uniporter (MCU) contributes to mitochondrial dysfunction and reactive oxygen species (ROS) production occurring upstream from the $Ca^{2+}$ deregulation, highlighting these events as potential targets for therapeutic intervention in ischemia.

## Materials and Methods

### Animals

Animal procedures were conducted in accordance with protocols approved by the Institutional Animal Care and Use Committee of the University of California at Irvine. Efforts were made to minimize animal suffering and number of mice used.

### Preparation of acute hippocampal slices

Hippocampal slices (300 μm) were prepared from 4 weeks old 129S6/SvEvTac mice (Taconic Farms, Inc) as previously described (Medvedeva et al., 2009). Briefly slices were cut with a vibratome (VT-1200, Leica Microsystems, Germany) in chilled cutting solution, containing (in mM): KCl 3, $NaH_2PO_4$ 1.25, $CaCl_2$ 0.2, $MgSO_4$ 6, $NaHCO_3$ 26, sucrose 220, glucose 10 and ketamine 0.43 (pH 7.35, 310 mOsm, equilibrated with 95% $O_2$/5% $CO_2$) and transferred into artificial cerebrospinal fluid (ACSF) containing (in mM): NaCl 126, KCl 3, $NaH_2PO_4$ 1.25, $CaCl_2$ 2, $MgSO_4$ 1, $NaHCO_3$ 26, and glucose 10 (pH 7.35, adjusted with sucrose to 310 mOsm and equilibrated with 95% $O_2$/5% $CO_2$) and incubated for 1 hour at 34°C.

### OGD exposures and low $[Ca^{2+}]_e$ experiments

To simulate hypoxic-hypoglycemic conditions, ACSF was replaced with identical solution but lacking glucose (glucose was substituted with an equimolar concentration of sucrose) and equilibrated with 95 % $N_2$ / 5% $CO_2$. For low $[Ca^{2+}]_e$ experiments, we prepared ACSF in which 1.8 mM $Ca^{2+}$ was substituted with $Mg^{2+}$ (thus containing 200 μM of $Ca^{2+}$ and 2.8 mM of $Mg^{2+}$).

### Loading individual hippocampal CA1 neurons with $Ca^{2+}$ and $Zn^{2+}$sensitive fluorescent indicators and fluorescence measurements

For recordings slices were placed in a flow-through chamber (RC-27L, Warner instruments; Hamden, CT) mounted on the stage of an upright microscope (BX51WI, Olympus, Japan) and superfused with oxygenated ACSF (95% $O_2$ / 5% $CO_2$) at 2 ml/min. Experiments were performed at 32±0.5μC.

For simultaneous measurements of intracellular $Ca^{2+}$ ($[Ca^{2+}]_i$) and $Zn^{2+}$ ($[Zn^{2+}]_i$) dynamics, cells were co-loaded with the low affinity $Ca^{2+}$ sensitive indicator Fura-6F ($K_{dCa}$~5.3 μM) or Fura-FF ($K_{dCa}$~5.5 μM), and the high affinity $Zn^{2+}$ sensitive indicator FluoZin-3 (Kd~15 nM) via patch pipettes as described previously (12). Fluorescent indicators were dissolved in pipette solution (containing (mM): 125 K Gluconate, 10 KCl, 3 Mg-ATP, 1 $MgCl_2$, 10 HEPES, pH 7.25 with KOH (290 mOsm with sucrose) to 1 mM, and a 1 μl droplet placed in pipette. Fluorescence was alternately excited at 340, 380 for Fura-6F or Fura-FF and 482 nm for FluoZin-3 (using 20 nm bandpass filters, Semrock Inc, USA) via a 40× water-immersion objective (numerical aperture 0.8, Olympus) and emission for both indicators collected at 532 (40) nm using a CCD camera (Hamamatsu, Japan). Images were acquired at 15 sec intervals and analyzed, after background subtraction, with METAFLUOR 7.1.7 software (Molecular Devices, Union City, CA). Changes in $[Ca^{2+}]_i$ are presented as the ratio of background subtracted emission intensities upon excitation at 340 and 380 nm (“340/380

ratio"), and $[Zn^{2+}]_i$ changes are presented as $\Delta F/F_0=(F_X-F_0$, where $F_X$ is the background subtracted fluorescence at each time point, x, and $F_0$ is the average background subtracted baseline fluorescence over the 10 min prior to OGD. The onset times of OGD-induced $Zn^{2+}$ rises and of $Ca^{2+}$ deregulations were determined by finding intersections between the extrapolated baselines, with lines fitting the first substantial FluoZin-3 fluorescence increases or Fura-6F ratio increases, as previously described (Medvedeva et al., 2009). To track ***membrane potential*** changes during OGD, the patch electrode was left attached to the CA1 neuron, and the potential was monitored in whole cell current clamp configuration.

### Measuring increase in reactive oxygen species (ROS) production evoked by OGD

To access changes in ROS production in response to OGD, we used the superoxide preferring ROS indicator, hydroethidine (HEt), which is oxidized into the highly fluorescent compound, ethidium. Slices were bath loaded with HEt (20 μM, 30 min at 22–25°C), subjected to OGD, and regions of interest were monitored in the CA1 pyramidal cell layer. HEt was exited at 540(25) nm and emitted fluorescence was collected at 605(55) nm. For simultaneously HEt and Fura-6F imaging, HEt was exited at 482(20) nm and emission collected at 532 (40) nm, resulting in some decrement in the fluorescence signal. Data are presented as $\Delta F/F_0=(F_X-F_0)/F_0$, where $F_X$ is the fluorescence at each time point, x, and $F_0$ is the baseline fluorescence, averaged over 5 min before OGD.

To quantify and compare ROS production across slices, the near linear sharply rising phase of each HEt ΔF trace (typically starting ~5–8 min and extending for 2–5 more min) was linearly fitted (to elicit a slope standard error, SE, <0.1; see Figure 3A), and the slope, ***m***, of this phase compiled across matched sets of control and treatment slices. Of note, whereas $Ca^{2+}$ deregulation times were quite closely reproducible across experimental animals and slice preparations, absolute HEt ΔF rise slopes were highly variable across slice sets, and for this reason all comparisons were made on matched sets of slices, with near equal (±1) numbers of control and treatment slices obtained from each preparation. Each set of slices was obtained from at least 3 animals.

### Reagents

Fura-6F, Fura-FF, FluorZin-3 and hydroethidine (dihydroethidium) were obtained from Invitrogen (Carlsbad, CA). RU360 was purchased from Calbiochem (EMD Biocsienses, La Jolla, CA), MK-801, Ruthenium Red, and N,N,N′,N′-Tetrakis(2-pyridylmethyl)ethylenediamine (TPEN) were obtained from Sigma (St. Louis, MO). Nimodipine was obtained from Miles Inc. (West Haven, CT). All other reagents were purchased from Fisher Scientific.

### Statistics

Data were analyzed using Origin 9.0 software. All differences between control and treatment groups were assessed by 2-tailed t tests.

## Results

### In physiological $Ca^{2+}$, MCU blockade accelerates $Ca^{2+}$ deregulation and cell death

To examine $Ca^{2+}$ and $Zn^{2+}$ changes in hippocampal CA1 pyramidal neurons during OGD, single neurons in acute slices were co-loaded with membrane impermeable forms of the high affinity $Zn^{2+}$ indicator FluoZin-3 ($K_d$ ~15 nM) and a low affinity $Ca^{2+}$ indicator (Fura-6F, $K_d$ ~ 5.3 μM; or Fura-FF, $K_d$ ~ 5.5 μM) via a patch pipette (see Materials and Methods). In our prior work, we found OGD evoked $Zn^{2+}$ rises to precede the sharp $Ca^{2+}$ rises (termed "$Ca^{2+}$ deregulations"). In addition, as discussed in the introduction, it was apparent that the $Ca^{2+}$ deregulation events were causatively linked to a terminal loss of membrane integrity. If $Zn^{2+}$ was chelated, the lethal $Ca^{2+}$ deregulation was delayed, and there was enhanced recovery of mitochondrial function, implicating a contribution of $Zn^{2+}$, likely in part via effects on mitochondria, to the terminal injury cascade (Medvedeva et al., 2009).

As neuronal depolarization is a well described early event in ischemic injury cascades, in order to better characterize our model, we sought to determine the relationship between the depolarization and the above described $Zn^{2+}$ and $Ca^{2+}$ rises. To do so, after indicator loading, we left the CA1 neuron in whole cell current clamp configuration to monitor membrane potential changes during OGD. In line with prior studies of depolarization of hippocampal neurons in slice during OGD (Yamamoto et al., 1997), we found depolarization to begin after ~ 6–7 min, shortly before the start of the cytosolic $Zn^{2+}$ rise, and well before the terminal $Ca^{2+}$ deregulation (Figure 1A).

The present study seeks to examine the specific contributions of $Ca^{2+}$ and $Zn^{2+}$ entry into mitochondria to the sequence of events leading to neurodegeneration during acute OGD. As the mitochondrial $Ca^{2+}$ uniporter (MCU) provides the primary route for $Ca^{2+}$ passage across the inner mitochondrial membrane into the matrix (Bernardi, 1999; Kirichok et al., 2004), and appears to permit $Zn^{2+}$ entry as well (Gazaryan et al., 2007; Jiang et al., 2001; Malaiyandi et al., 2005; Saris and Niva, 1994), we next examined effects of MCU blockade. When 10 μM of the MCU blocker, Ruthenium Red (RR) (Moore, 1971) was added to the extracellular buffer prior to and during a 15 min OGD episode, the $Ca^{2+}$ deregulation was accelerated (occurring after 8.7±0.53 min vs 11.5±0.4 in control; Figure 1B). Since mitochondria are important high capacity buffers of intracellular $Ca^{2+}$ loads, we considered whether block of mitochondrial $Ca^{2+}$ uptake by RR might directly facilitate the occurrence of the lethal cytosolic $Ca^{2+}$ deregulation, thus obscuring the ability to resolve effects of mitochondrial $Zn^{2+}$ uptake. For this reason, we examined the effect of adding blockers of two major routes of $Ca^{2+}$ entry: N-methyl-D-aspartate (NMDA) channels and voltage gated $Ca^{2+}$ channels (VGCC). Since we expected the presence of these channel blockers would delay the onset of $Ca^{2+}$ deregulation, in these experiments, the OGD duration was increased to 25 min. Addition of the NMDA channel blocker MK-801 (10 μM) and the VGCC blocker nimodipine (10 μM) during OGD modestly delayed the time of the $Ca^{2+}$ deregulation (to 16.4±1.0 min from 11.5±0.4 in control; Figure 1C). Moreover, similar to the results obtained in the absence of the $Ca^{2+}$ entry blockers (Medvedeva et al., 2009), $Zn^{2+}$ chelation with the high affinity membrane permeable $Zn^{2+}$ chelator TPEN (40 μM) further delayed the $Ca^{2+}$ deregulation (to 22.7±1.5 min; Figure 1C). And finally, when cytosolic $Ca^{2+}$ loading was

decreased by the $Ca^{2+}$ entry blockers, further MCU inhibition with RR had the opposite effect as seen without blockers, significantly delaying the $Ca^{2+}$ deregulation to a similar degree as $Zn^{2+}$ chelation with TPEN (to 21.9±1.61 min; Figure 1D), consistent with our hypothesis that rapid cytoplasmic $Ca^{2+}$ accumulation in the presence of RR precluded the ability to resolve possible beneficial effects of MCU blockade, such as inhibition of mitochondrial $Zn^{2+}$ uptake.

Thus, to simplify the paradigm and avoid possible complications due to variable tissue penetrance or non-specific effects of the $Ca^{2+}$ entry blockers, we next carried out experiments in which, instead of adding MK-801 and nimodipine, slices were bathed in artificial cerebrospinal fluid (ACSF) buffer in which the $Ca^{2+}$ concentration ($[Ca^{2+}]_e$) was lowered from a physiological level (2 mM) to 200 μM. Under these conditions, $Ca^{2+}$ deregulation was substantially delayed (to 19.4±1.26 min; Figure 2A). Similar to the results observed in 2 mM $[Ca^{2+}]_e$ in the absence (Medvedeva et al., 2009) or presence (Figure 1C) of $Ca^{2+}$ channels blockers, $Zn^{2+}$ chelation with TPEN resulted in a significant further delay of the $Ca^{2+}$ deregulation (to 27.4±0.47 min; Figure 2A), indicating that in low $[Ca^{2+}]_e$, $Zn^{2+}$ still significantly contributes to the neurodegenerative cascade.

Furthermore, with 200 μM $[Ca^{2+}]_e$, MCU blockade with RR had a similar effect to that seen in 2 mM $[Ca^{2+}]_e$ with $Ca^{2+}$ entry blockers, markedly delaying the $Ca^{2+}$ deregulation (to 34.1±1.81 min; Figure 2B,E). Since, in these experiments, $Ca^{2+}$ deregulation occurred well after the end of the 25 min OGD episode, we carried out a set of experiments in which OGD was extended beyond the onset of $Ca^{2+}$ deregulation ("continuous OGD"), and, as expected, MCU inhibition still substantially delayed the $Ca^{2+}$ deregulation (to 28.9.1±2.1min; see supplemental Figure S1). Although RR is a widely used MCU blocker, it is not completely selective, also having effects on other cellular channels (Tapia and Velasco, 1997). Therefore, to further confirm the neuroprotective effects of MCU inhibition against OGD induced neuronal injury in low $[Ca^{2+}]_e$ conditions, experiments were repeated using the more selective RR derivative, RU360 (Matlib et al., 1998). For these studies, as RU360 is highly oxidation sensitive and unstable in solution, rather than bath loading the slice, RU360 was mixed with deoxygenated intracellular solution just prior to use, and introduced directly into the selected CA1 pyramidal neuron via the patch electrode along with fluorescent indicators. RU360 had similar protective effect as observed with bath application of RR (delaying $Ca^{2+}$ deregulation to 34.25±4.9 min; Figure 2C, E).

We wondered whether the protective effects of MCU blockers against OGD induced $Ca^{2+}$ deregulation in low $[Ca^{2+}]_e$ might be due to blockade of $Zn^{2+}$ entry into mitochondria. Consistent with this idea, the presence of RR during OGD in low $[Ca^{2+}]_e$ ACSF not only reproduced (and modestly exceeded) the protective effect of TPEN, but also accelerated the onset of cytosolic $Zn^{2+}$ rises (to 5.8±0.5 min vs 8.3±0.9 min in control; Figure 2 D,E).

## $Zn^{2+}$ contributes to OGD induced ROS generation

Despite strong evidence that ROS generation contributes to ischemic neuronal injury (Chan, 2001; Kuroda and Siesjo, 1997), dynamics of ischemia-associated ROS generation have been little studied. Thus, in subsequent studies we utilized the superoxide preferring ROS indicator, hydroethidine (HEt) (Bindokas et al., 1996; Carriedo et al., 1998) to examine

contributions of $Ca^{2+}$ and $Zn^{2+}$ to OGD induced ROS generation. In the presence of ROS, HEt is oxidized into highly fluorescent ethidium; the rate of HEt fluorescence increase (HEt ΔF) provides a measure of the ROS generation rate. After bath loading with HEt, slices were placed in the recording chamber and subjected to OGD (15 min). A slow acceleration of HEt ΔF typically occurred after ~ 1–3 min with a marked acceleration in ΔF occurring slightly later (typically between 5 and 9 min); a steep linear ΔF rise typically lasted for 2–5 more minutes (Figure 3), before slowing due to pronounced cellular swelling. To quantify and compare rates of HEt ΔF rise, slopes (***m***) of these steep phases in the HEt ΔF rise were obtained through linear fitting (see Materials and Methods; Figure 3A). In both high and low $[Ca^{2+}]_e$, the HEt ΔF rise preceded the $Ca^{2+}$ deregulation (supplemental Figure S2). Despite the marked delay in the time of $Ca^{2+}$ deregulation, when $[Ca^{2+}]_e$ was lowered to 200 μM, the HEt ΔF was distinctly altered, rising more sharply compared to that in presence of 2 mM $Ca^{2+}$ (to $\boldsymbol{m}$ = 4.26±0.35 vs 3.22±0.34 in 2 mM $[Ca^{2+}]_e$; Figure 3B). To examine possible contributions of $Zn^{2+}$ to ROS generation, identical exposures were carried out in the presence of TPEN.

$Zn^{2+}$ chelation has relatively little effect on fluorescence increases in 2 mM $[Ca^{2+}]_e$ (supplemental Figure S3). However, it may be difficult to resolve contribution of $Zn^{2+}$ to ROS generation under these conditions, since strong $Ca^{2+}$ loading has been well documented to induce ROS production from extra-mitochondrial as well as mitochondrial sources. In contrast, when OGD was carried out in low $[Ca^{2+}]_e$, addition of TPEN significantly decreased the slope of the steep HEt ΔF (to $\boldsymbol{m}$ = 6.42±0.41 from 9.82±0.82 in control; Figure 3C).

These observations indicate that $Zn^{2+}$ makes a greater contribution to acute OGD induced ROS generation if the $[Ca^{2+}]_e$ is lowered, suggesting that $Ca^{2+}$ has an inhibitory effect on this $Zn^{2+}$ dependent ROS generation. $Ca^{2+}$ inhibition of $Zn^{2+}$ dependent ROS generation could be most readily explained if there were competition between these ions for some site upstream from the $Zn^{2+}$ triggered ROS release. One such site could be the MCU, with high levels of $Ca^{2+}$ interfering with the passage of $Zn^{2+}$ through this channel.

To test the role of the MCU in the OGD induced ROS generation, we first investigated effects of RR on HEt ΔF during OGD carried out in 2 mM $[Ca^{2+}]_e$. RR application markedly slowed the ROS production (Figure 3D). However, as RR accelerated $Ca^{2+}$ deregulation and cell death in 2 mM $[Ca^{2+}]_e$, HEt recording could not be carried out beyond 8–10 min. In addition, since high $[Ca^{2+}]_e$ was present during the OGD, it is not apparent whether the effects of RR are more due to block of $Ca^{2+}$ and/or of $Zn^{2+}$ entry through the MCU. For this reason, we next examined effects of RR on slices subjected to OGD in low $[Ca^{2+}]_e$. Addition of RR markedly slowed the steep phase of the HEt ΔF, with effects that were qualitatively similar to but greater than those caused by TPEN (to $\boldsymbol{m}$ = 1.96±0.33 vs 4.1± 0.5 in control; Figure 3E). The greater efficacy of RR than TPEN on the ROS production could reflect combined block of $Ca^{2+}$ as well as of $Zn^{2+}$ entry into mitochondria. This is likely consistent with our prior observations demonstrating synergistic effects of exogenous $Ca^{2+}$ and $Zn^{2+}$ loading on ROS production in cultured neurons (Sensi et al., 2000), and on swelling of isolated mitochondria (Jiang et al., 2001). If the effects of RR on ROS generation reflected only attenuation of $Ca^{2+}$ entry and were independent of $Zn^{2+}$, we would

expect to see additive attenuation of ROS generation when slices were treated with TPEN as well as RR. However, when experiments were performed with simultaneous TPEN and RR exposure, the decrease in the HEt ΔF slope was no greater than with RR alone, providing strong evidence that the effect of RR is at least in part due to block of $Zn^{2+}$ entry into the mitochondrial matrix through the MCU (Figure 3F).

## Discussion

Despite strong evidence for contributions of both $Ca^{2+}$ and $Zn^{2+}$ loading in ischemic neurodegeneration (Medvedeva et al., 2009; Randall and Thayer, 1992; Vander Jagt et al., 2008), our understanding of the respective contributions of these two cations has been limited, in part because of difficulties distinguishing these ions. Indeed, as the widely used fluorescent $Ca^{2+}$ indicators are all also responsive to $Zn^{2+}$ with greater molar potency than $Ca^{2+}$, it is likely that some effects previously attributed to $Ca^{2+}$ are in fact $Zn^{2+}$ mediated (Stork and Li, 2006). The advent of good $Zn^{2+}$ selective fluorescent indicators combined with use of $Zn^{2+}$ chelators has enabled simultaneous detection of these cations and new investigations of their respective contributions (Devinney et al., 2005; Medvedeva et al., 2009). In recent studies of acute hippocampal slices subjected to OGD we documented the occurrence of early cytosolic $Zn^{2+}$ rises that appeared to contribute to the onset of subsequent "$Ca^{2+}$ deregulation" events, which were causatively linked to a terminal loss of membrane integrity and cell death (Medvedeva et al., 2009).

It is apparent that mitochondria serve as important buffers for large cytosolic $Ca^{2+}$ loads, reflecting uptake into the polarized mitochondrial matrix via the MCU (Wang and Thayer, 1996; Wang and Thayer, 2002), and numerous studies have reported $Ca^{2+}$ overloading to induce mitochondrial dysfunction. However, as discussed in results, $Zn^{2+}$ can also permeate the MCU, and appears to trigger effects including mitochondrial depolarization, ROS generation and swelling, apparently due to mitochondrial permeability transition pore (mPTP) induction, with far greater molar potency than $Ca^{2+}$ (Gazaryan et al., 2007; Jiang et al., 2001; Sensi et al., 1999; Sensi et al., 2003; Wudarczyk et al., 1999). Suggesting that mitochondrial $Zn^{2+}$ entry could contribute to injury, RR decreased both the ROS generation and neuronal injury caused by application of $Zn^{2+}$ to cultured neurons (Clausen et al., 2013; Lozier et al., 2012).

Whereas above studies examined effects of exogenous $Zn^{2+}$, neuronal $Zn^{2+}$ accumulation during ischemia likely reflects a combination of trans-synaptic passage of synaptically released $Zn^{2+}$, and $Zn^{2+}$ release from cytosolic buffering proteins like metallothioneins (due to ischemia associated oxidative stress and acidosis) (Shuttleworth and Weiss, 2011), and emerging evidence suggests that this endogenous $Zn^{2+}$ mobilization can also impact mitochondria. Indeed, endogenous $Zn^{2+}$ accumulation appears to contribute to opening of channels in mitochondrial membranes and release of apoptotic mediators from mitochondria after *in vivo* ischemia (Bonanni et al., 2006; Calderone et al., 2004). We have found that oxidant induced mobilization of endogenous $Zn^{2+}$ can cause mitochondrial depolarization of cultured neurons (Sensi et al., 2003), and that early $Zn^{2+}$ accumulation appears to contribute to irreversible mitochondrial depolarization in hippocampal slices subjected to OGD (Medvedeva et al., 2009).

The primary goal of present studies was to use MCU blockers to gain insights into the specific contribution of $Zn^{2+}$ entry into mitochondria through these channels in acute ischemic neurodegeneration. Of note, prior studies using MCU blockers have yielded divergent effects, protecting isolated mitochondria from hypoxic injury (Schild et al., 2003), but having either beneficial effects, or deleterious effects associated with cytosolic $Ca^{2+}$ overload in both neuronal and cardiac tissues depending upon the precise paradigm employed (Figueredo et al., 1991; Ruiz-Meana et al., 2006; Velasco and Tapia, 2000; Zhao et al., 2013). In line with these observations, we find that addition of RR during OGD carried out in physiological $[Ca^{2+}]_e$ in the absence of $Ca^{2+}$ entry blockers accelerated the $Ca^{2+}$ deregulation (Figure 1B), likely by interfering with the ability of mitochondria to buffer large cytosolic $Ca^{2+}$ loads, and possibly obscuring the ability to resolve beneficial effects of blocking mitochondrial $Zn^{2+}$ entry. Supporting this interpretation, when $Ca^{2+}$ entry was slowed, either by addition of $Ca^{2+}$ entry blockers or by lowering the $[Ca^{2+}]_e$, MCU blockade accelerated the cytosolic $Zn^{2+}$ rise (Figure 2D,E), while significantly delaying the $Ca^{2+}$ deregulation to a similar degree as $Zn^{2+}$ chelation (Figure 1C,D; Figure 2AB,C). Thus, while prior studies have indicated that endogenous $Zn^{2+}$ can affect mitochondria, present observations that under conditions of attenuated $Ca^{2+}$ entry, either $Zn^{2+}$ chelation or MCU blockade is markedly protective provides new support for the hypothesis that passage of $Zn^{2+}$ into mitochondria through the MCU is an early event in the neuronal injury cascade.

Interestingly, most studies of ischemic ROS generation have focused on the reperfusion phase, and although ROS production has been observed during OGD in both culture and slice models (Abramov et al., 2007; Frantseva et al., 2001), this has been relatively little studied. Using HEt to image ROS generation in CA1 neurons during OGD reveals a distinct increase in fluorescence (ΔF) beginning shortly after OGD onset (Figure 3A). Whereas multiple studies have reported that large intracellular $Ca^{2+}$ loads can trigger mitochondrial ROS release (Bindokas et al., 1996; Carriedo et al., 1998; Dugan et al., 1995; Reynolds and Hastings, 1995), effects of $Ca^{2+}$ on mitochondria are complex, and mechanisms of $Ca^{2+}$ dependent enhancement of mitochondrial ROS release are poorly understood (Adam-Vizi and Starkov, 2010; Feissner et al., 2009; Peng and Jou, 2010). In the present studies, we were surprised to find that lowering $Ca^{2+}$, despite delaying the $Ca^{2+}$ deregulation, actually accelerated the ROS generation (Figure 3B). This observation provides evidence against the contention that $Ca^{2+}$ loading is the only critical trigger of the ROS generation, and, taken together with observations that the ROS production was attenuated non-additively by either $Zn^{2+}$ chelation or MCU blockade (Figure 3C,E,F), lends new support for the idea that $Zn^{2+}$ entry into mitochondria via the MCU is contributory.

Whereas it is clear that exogenous $Zn^{2+}$ loading can trigger mitochondrial ROS generation (Sensi et al., 1999), present observations support the idea that endogenous $Zn^{2+}$ does so as well. First, it is apparent that $Zn^{2+}$ effects are not due simply to direct depolarization of mitochondria as a consequence of the charge carried by the $Zn^{2+}$ entry, since absolute far greater levels of intracellular $Ca^{2+}$, which readily enters polarized mitochondria through the MCU, have less effect. Mechanisms of $Zn^{2+}$ dependent mitochondrial ROS generation are uncertain, but like $Ca^{2+}$, there is evidence that it can induce block of the electron transport chain (Link and von Jagow, 1995; Skulachev et al., 1967), and can promote opening of the

mPTP (Jiang et al., 2001; Wudarczyk et al., 1999), possibly after inducing potent (nM) and irreversible inhibition of key mitochondrial enzymes with critical roles in energy production and antioxidant defense (Gazaryan et al., 2007). In light of present observations that lowering $[Ca^{2+}]_e$ results in increased $Zn^{2+}$ dependent ROS generation, might $Zn^{2+}$ actually be the more significant of these endogenous cations in the induction of mitochondrial ROS generation during ischemia?

### Conclusions / clinical implications

Stroke presents extreme therapeutic challenges, reflecting both difficulties in rapid delivery of therapeutic interventions to ischemic brain and incomplete understanding of critical pathophysiological events. Despite longstanding interest in contributions of $Ca^{2+}$, therapeutics targeting $Ca^{2+}$ have yielded limited benefit, while further studies have highlighted important but poorly defined contributions of $Zn^{2+}$. These $Zn^{2+}$ dependent effects are likely of particular importance in conditions like ischemia, wherein oxidative stress and acidosis impair cytosolic $Zn^{2+}$ buffering, such that modest cytosolic loading may result in uptake into and disruption of mitochondrial function including ROS generation (Clausen et al., 2013; Sensi et al., 2003). The emerging understanding of potent interactions of $Zn^{2+}$ with mitochondria in early phases of ischemia/OGD suggests mechanisms that may contribute to early stages in the cell death cascade. Specifically, mitochondrial $Zn^{2+}$ uptake might hasten events including metabolic failure and ROS generation, resulting in the cell losing its ability to maintain $Ca^{2+}$ ionic homeostasis, with the result that $Ca^{2+}$ deregulation occurs, triggering catastrophic cell damage including loss of membrane integrity, likely in large part via activation of catabolic enzymes. Furthermore, we suggest that these events, if appropriately targeted, have the potential to delay the onset of energy failure occurring upstream to the occurrence of irreversible injury.

Although present results support an early role of mitochondrial $Zn^{2+}$ entry through the MCU in these events, since MCU blockade may itself promote increased cytosolic $Ca^{2+}$ and $Zn^{2+}$ loading, MCU blockers alone may not prove effective against acute ischemic injury. Perhaps optimal interventions will use other approaches to either diminish $Zn^{2+}$ accumulation within mitochondria, or protect mitochondria from the deleterious effects of $Zn^{2+}$. Alternatively, MCU blockers might prove to be effective when combined with other interventions that either diminish the magnitude of the $Ca^{2+}$ load (as suggested by present observations using $Ca^{2+}$ entry blockers), or antagonize the injurious effects of cytosolic $Ca^{2+}$ or $Zn^{2+}$ loads (like inhibitors of $Ca^{2+}$ dependent catabolic enzymes or $Zn^{2+}$ dependent signaling cascades) (Shuttleworth and Weiss, 2011). It is hoped that with the right set of interventions, early $Zn^{2+}$ dependent mitochondrial dysfunction can be abrogated, permitting greater opportunity for recovery from brain ischemia.

## Supplementary Material

Refer to Web version on PubMed Central for supplementary material.

## Acknowledgments

Supported by NIH grants T32 NS45540 (Y.V.M), R01 NS065219 (J.H.W.). We thank Jenny Truong for excellent help with animal care and breeding.

## References

Abramov AY, Scorziello A, Duchen MR. Three distinct mechanisms generate oxygen free radicals in neurons and contribute to cell death during anoxia and reoxygenation. J Neurosci. 2007; 27:1129–1138. [PubMed: 17267568]

Adam-Vizi V, Starkov AA. Calcium and mitochondrial reactive oxygen species generation: how to read the facts. J Alzheimers Dis. 2010; 20(Suppl 2):S413–S426. [PubMed: 20421693]

Bernardi P. Mitochondrial transport of cations: channels, exchangers, and permeability transition. Physiol Rev. 1999; 79:1127–1155. [PubMed: 10508231]

Bindokas VP, et al. Superoxide production in rat hippocampal neurons: selective imaging with hydroethidine. J Neurosci. 1996; 16:1324–1336. [PubMed: 8778284]

Bonanni L, et al. Zinc-dependent multi-conductance channel activity in mitochondria isolated from ischemic brain. J Neurosci. 2006; 26:6851–6862. [PubMed: 16793892]

Calderone A, et al. Late calcium EDTA rescues hippocampal CA1 neurons from global ischemia-induced death. J Neurosci. 2004; 24:9903–9913. [PubMed: 15525775]

Carriedo SG, et al. Rapid Ca2+ entry through Ca2+-permeable AMPA/Kainate channels triggers marked intracellular Ca2+ rises and consequent oxygen radical production. J Neurosci. 1998; 18:7727–7738. [PubMed: 9742143]

Carter RE, et al. Spreading depression and related events are significant sources of neuronal Zn2+ release and accumulation. J Cereb Blood Flow Metab. 2011; 31:1073–1084. [PubMed: 20978516]

Chan PH. Reactive oxygen radicals in signaling and damage in the ischemic brain. J Cereb Blood Flow Metab. 2001; 21:2–14. [PubMed: 11149664]

Clausen A, et al. Mechanisms of Rapid Reactive Oxygen Species Generation in response to Cytosolic Ca2+ or Zn2+ Loads in Cortical Neurons. Plos One. 2013; 8:e83347. [PubMed: 24340096]

Devinney MJ, Reynolds IJ 2nd, Dineley KE. Simultaneous detection of intracellular free calcium and zinc using fura-2FF and FluoZin-3. Cell Calcium. 2005; 37:225–232. [PubMed: 15670869]

Dineley KE, Votyakova TV, Reynolds IJ. Zinc inhibition of cellular energy production: implications for mitochondria and neurodegeneration. J Neurochem. 2003; 85:563–570. [PubMed: 12694382]

Dugan LL, et al. Mitochondrial production of reactive oxygen species in cortical neurons following exposure to N-methyl-D-aspartate. J Neurosci. 1995; 15:6377–6388. [PubMed: 7472402]

Feissner RF, et al. Crosstalk signaling between mitochondrial Ca2+ and ROS. Front Biosci. 2009; 14:1197–1218.

Figueredo VM, et al. Postischaemic reperfusion injury in the isolated rat heart: effect of ruthenium red. Cardiovasc Res. 1991; 25:337–342. [PubMed: 1715813]

Frantseva MV, Carlen PL, Perez Velazquez JL. Dynamics of intracellular calcium and free radical production during ischemia in pyramidal neurons. Free Radic Biol Med. 2001; 31:1216–1227. [PubMed: 11705700]

Frederickson CJ, Hernandez MD, McGinty JF. Translocation of zinc may contribute to seizure-induced death of neurons. Brain Res. 1989; 480:317–321. [PubMed: 2713657]

Gazaryan IG, et al. Zinc irreversibly damages major enzymes of energy production and antioxidant defense prior to mitochondrial permeability transition. J Biol Chem. 2007; 282:24373–24380. [PubMed: 17565998]

Jiang D, et al. Zn(2+) induces permeability transition pore opening and release of proapoptotic peptides from neuronal mitochondria. J Biol Chem. 2001; 276:47524–47529. [PubMed: 11595748]

Kirichok Y, Krapivinsky G, Clapham DE. The mitochondrial calcium uniporter is a highly selective ion channel. Nature. 2004; 427:360–364. [PubMed: 14737170]

Koh JY, et al. The role of zinc in selective neuronal death after transient global cerebral ischemia. Science. 1996; 272:1013–1016. [PubMed: 8638123]

Kuroda S, Siesjo BK. Reperfusion damage following focal ischemia: pathophysiology and therapeutic windows. Clin Neurosci. 1997; 4:199–212. [PubMed: 9186042]

Link TA, von Jagow G. Zinc ions inhibit the QP center of bovine heart mitochondrial bc1 complex by blocking a protonatable group. J Biol Chem. 1995; 270:25001–25006. [PubMed: 7559629]

Lozier ER, et al. Stimulation of kainate toxicity by zinc in cultured cerebellar granule neurons and the role of mitochondria in this process. Toxicol Lett. 2012; 208:36–40. [PubMed: 22008730]

Malaiyandi LM, et al. Direct visualization of mitochondrial zinc accumulation reveals uniporter-dependent and -independent transport mechanisms. J Neurochem. 2005; 93:1242–1250. [PubMed: 15934944]

Matlib MA, et al. Oxygen-bridged dinuclear ruthenium amine complex specifically inhibits Ca2+ uptake into mitochondria in vitro and in situ in single cardiac myocytes. J Biol Chem. 1998; 273:10223–10231. [PubMed: 9553073]

Medvedeva YV, et al. Intracellular Zn2+ accumulation contributes to synaptic failure, mitochondrial depolarization, and cell death in an acute slice oxygen-glucose deprivation model of ischemia. J Neurosci. 2009; 29:1105–1114. [PubMed: 19176819]

Moore CL. Specific inhibition of mitochondrial Ca++ transport by ruthenium red. Biochem Biophys Res Commun. 1971; 42:298–305. [PubMed: 4250976]

Peng TI, Jou MJ. Oxidative stress caused by mitochondrial calcium overload. Ann N Y Acad Sci. 2010; 1201:183–188. [PubMed: 20649555]

Randall RD, Thayer SA. Glutamate-induced calcium transient triggers delayed calcium overload and neurotoxicity in rat hippocampal neurons. J Neurosci. 1992; 12:1882–1895. [PubMed: 1349638]

Reynolds IJ, Hastings TG. Glutamate induces the production of reactive oxygen species in cultured forebrain neurons following NMDA receptor activation. J Neurosci. 1995; 15:3318–3327. [PubMed: 7751912]

Rothman SM, Olney JW. Glutamate and the pathophysiology of hypoxic--ischemic brain damage. Ann Neurol. 1986; 19:105–111. [PubMed: 2421636]

Ruiz-Meana M, et al. Mitochondrial Ca2+ uptake during simulated ischemia does not affect permeability transition pore opening upon simulated reperfusion. Cardiovasc Res. 2006; 71:715–724. [PubMed: 16860295]

Saris NE, Niva K. Is Zn2+ transported by the mitochondrial calcium uniporter? FEBS Lett. 1994; 356:195–198. [PubMed: 7528685]

Schild L, et al. Brain mitochondria are primed by moderate Ca2+ rise upon hypoxia/reoxygenation for functional breakdown and morphological disintegration. J Biol Chem. 2003; 278:25454–25460. [PubMed: 12702720]

Sensi SL, et al. Preferential Zn2+ influx through Ca2+-permeable AMPA/kainate channels triggers prolonged mitochondrial superoxide production. Proc Natl Acad Sci U S A. 1999; 96:2414–2419. [PubMed: 10051656]

Sensi SL, Yin HZ, Weiss JH. AMPA/kainate receptor-triggered Zn2+ entry into cortical neurons induces mitochondrial Zn2+ uptake and persistent mitochondrial dysfunction. Eur J Neurosci. 2000; 12:3813–3818. [PubMed: 11029652]

Sensi SL, et al. Modulation of mitochondrial function by endogenous Zn2+ pools. Proc Natl Acad Sci U S A. 2003; 100:6157–6162. [PubMed: 12724524]

Shuttleworth CW, Weiss JH. Zinc: new clues to diverse roles in brain ischemia. Trends Pharmacol Sci. 2011; 32:480–486. [PubMed: 21621864]

Siesjo BK. Historical overview. Calcium, ischemia, and death of brain cells. Ann N Y Acad Sci. 1988; 522:638–661. [PubMed: 2454060]

Skulachev VP, et al. Inhibition of the respiratory chain by zinc ions. Biochem Biophys Res Commun. 1967; 26:1–6. [PubMed: 4291553]

Stork CJ, Li YV. Intracellular zinc elevation measured with a"calcium-specific" indicator during ischemia and reperfusion in rat hippocampus: a question on calcium overload. J Neurosci. 2006; 26:10430–10437. [PubMed: 17035527]

Tapia R, Velasco I. Ruthenium red as a tool to study calcium channels, neuronal death and the function of neural pathways. Neurochem Int. 1997; 30:137–147. [PubMed: 9017661]

Tonder N, et al. Possible role of zinc in the selective degeneration of dentate hilar neurons after cerebral ischemia in the adult rat. Neurosci Lett. 1990; 109:247–252. [PubMed: 2330128]

Vander Jagt TA, Connor JA, Shuttleworth CW. Localized loss of Ca2+ homeostasis in neuronal dendrites is a downstream consequence of metabolic compromise during extended NMDA exposures. J Neurosci. 2008; 28:5029–5039. [PubMed: 18463256]

Velasco I, Tapia R. Alterations of intracellular calcium homeostasis and mitochondrial function are involved in ruthenium red neurotoxicity in primary cortical cultures. J Neurosci Res. 2000; 60:543–551. [PubMed: 10797557]

Wang GJ, Thayer SA. Sequestration of glutamate-induced Ca2+ loads by mitochondria in cultured rat hippocampal neurons. J Neurophysiol. 1996; 76:1611–1621. [PubMed: 8890280]

Wang GJ, Thayer SA. NMDA-induced calcium loads recycle across the mitochondrial inner membrane of hippocampal neurons in culture. J Neurophysiol. 2002; 87:740–749. [PubMed: 11826043]

Wei G, et al. Characterization of extracellular accumulation of Zn2+ during ischemia and reperfusion of hippocampus slices in rat. Neuroscience. 2004; 125:867–877. [PubMed: 15120848]

Weiss JH, Sensi SL, Koh JY. Zn(2+): a novel ionic mediator of neural injury in brain disease. Trends Pharmacol Sci. 2000; 21:395–401. [PubMed: 11050320]

Wudarczyk J, Debska G, Lenartowicz E. Zinc as an inducer of the membrane permeability transition in rat liver mitochondria. Arch Biochem Biophys. 1999; 363:1–8. [PubMed: 10049493]

Yamamoto S, et al. Factors that reverse the persistent depolarization produced by deprivation of oxygen and glucose in rat hippocampal CA1 neurons in vitro. J Neurophysiol. 1997; 78:903–911. [PubMed: 9307123]

Yin HZ, et al. Blockade of Ca2+-permeable AMPA/kainate channels decreases oxygenglucose deprivation-induced Zn2+ accumulation and neuronal loss in hippocampal pyramidal neurons. J Neurosci. 2002; 22:1273–1279. [PubMed: 11850455]

Zhao Q, et al. The role of the mitochondrial calcium uniporter in cerebral ischemia/reperfusion injury in rats involves regulation of mitochondrial energy metabolism. Mol Med Rep. 2013; 7:1073–1080. [PubMed: 23426506]

## Highlights

- During slice ischemia, early $Zn^{2+}$ rises contribute to the neurodegenerative cascade
- These effects of $Zn^{2+}$ are triggered by mitochondrial $Zn^{2+}$ entry via the MCU
- Mitochondrial $Zn^{2+}$ uptake contributes importantly to acute ischemic ROS production
- Mitochondrial $Zn^{2+}$ uptake may be an attractive target for ischemic neuroprotection

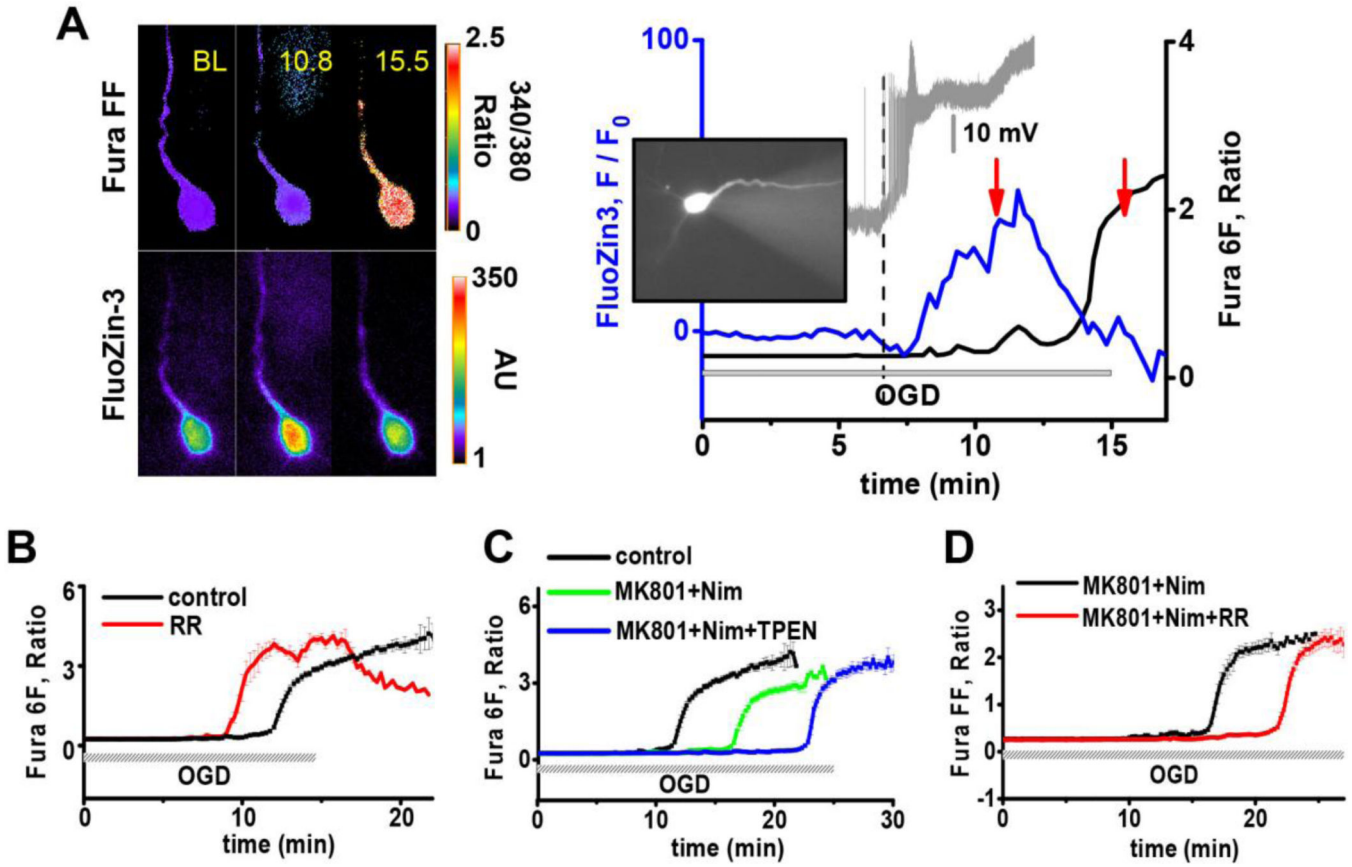


**Figure 1. $Zn^{2+}$ and $Ca^{2+}$ both contribute to OGD evoked neuronal injury**

Individual CA1 neurons were co-loaded with low affinity ratiometric $Ca^{2+}$ indicators Fura-FF (A,D) or Fura-6F (B,C) and the $Zn^{2+}$ sensitive indicator FluoZin-3, and the slices were subjected to OGD.

**A:** Relationship between plasma membrane depolarization and intracellular $Zn^{2+}$ and $Ca^{2+}$ rises in an individual CA1 neuron subjected to OGD. **Left:** Pseudocolor fluorescent images of a CA1 neuron co-loaded with Fura-FF (top, 340/380 ratio images) and FluoZin-3 (bottom, background subtracted emission intensity, arbitrary units) and subjected to 15 min OGD. Numbers indicate time (in min) following the onset of OGD (BL = base line). **Right:** Traces show changes in membrane potential (**grey**), FluoZin-3 fluorescence (**blue**) and Fura-FF ratio (**black**) in the CA1 neuron. Insert show fluorescent image (Ex: 380 nm) to display the cytosolic distribution of the Fura-FF (the gray triangle to the right is an artifact of the attached patch pipette). Arrows indicate time points (10.8 and 15.5 min) of the images shown **(Left)**. Note that the membrane depolarization (occurring after 6.7±0.3 min, n=3) begins shortly before the $Zn^{2+}$ rise, and that the $Zn^{2+}$ rise precedes the $Ca^{2+}$ deregulation. **B–D**: All traces depict mean Fura-6F 340/380 ratio changes (±SEM), and, for clarity of display, are aligned for the onset of $Ca^{2+}$ deregulation. OGD bars show approximate start and end time of the OGD episode, reflecting mild variations in the precise $Ca^{2+}$ deregulation times in different slices. **B:** In physiological (2 mM) $[Ca^{2+}]_e$, the mitochondrial $Ca^{2+}$ uniporter (MCU) blocker, Ruthenium Red (RR) accelerates OGD evoked $Ca^{2+}$ deregulation. Slices were subjected to OGD alone or with RR (10 μM, 15 min prior to and during the 15

min OGD episode). ($Ca^{2+}$ deregulation occurred after 11.5±0.4 min in control, **black**, n=10; vs 8.7±0.53 min with RR, **red**, n=10; $p<0.005$). **C:** $Ca^{2+}$ entry blockers and $Zn^{2+}$ chelation additively delay OGD evoked $Ca^{2+}$ deregulation. Combined application of the NMDA receptor blocker MK-801 (10 μM) and the VGCC blocker nimodipine (10 μM) delays $Ca^{2+}$ deregulation (from 11.5±0.4, n=10, **black**, in control to 16.4±1.0, n=9, **green**, with blockers, $p<0.005$), and $Ca^{2+}$ deregulation is further delayed by addition of the $Zn^{2+}$ chelator TPEN (to 22.7±1.5, n=8, **blue**, $p<0.005$ vs blockers alone). All drugs were applied 10 min prior to and during the OGD episode. **D:** In the presence of MK-801 and nimodipine, RR delays $Ca^{2+}$ deregulation (from 16.3±1.34 min, n=7, **black,** in presence of blockers alone to 21.9±1.61min, n=9, **red**, with blockers and RR, $p<0.05$). RR was applied 15 min prior to and during 25 min OGD episode.

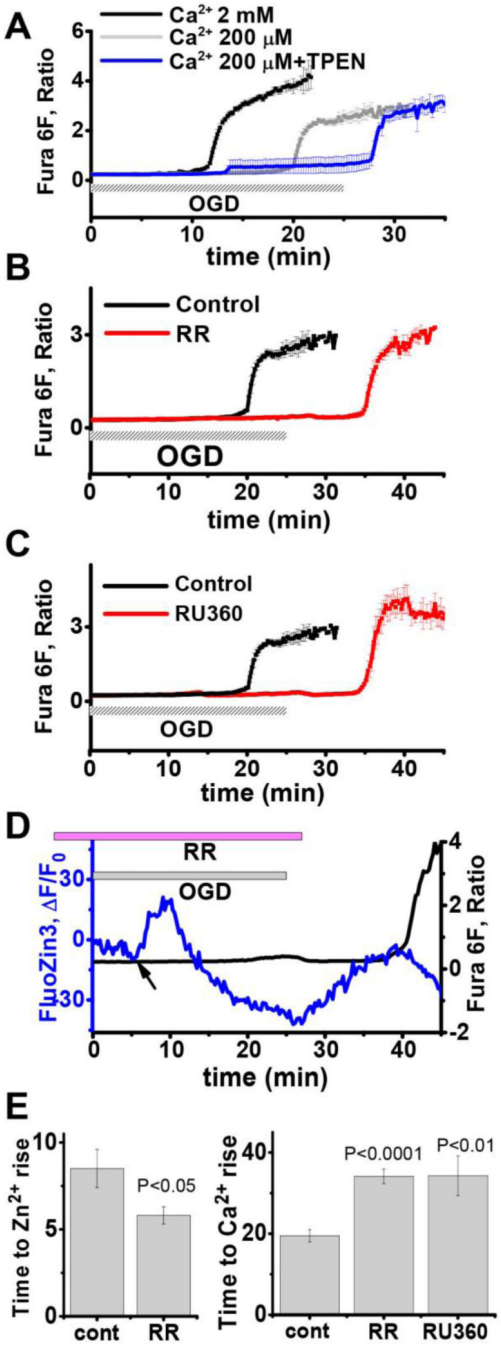


**Figure 2. In low $[Ca^{2+}]_e$, either $Zn^{2+}$ chelation or MCU inhibition delays OGD evoked $Ca^{2+}$ deregulation**

Individual CA1 neurons were loaded with Fura-6F and FluoZin-3 as described and subjected to a 25 min episode of OGD in 200 μM $[Ca^{2+}]_e$.

**A**: Decreasing $[Ca^{2+}]_e$ to 200 μM and $Zn^{2+}$ chelation additively delay OGD evoked $Ca^{2+}$ deregulation. Slices were subjected to OGD in 2 mM $[Ca^{2+}]_e$ (**black**), or in 200 μM $[Ca^{2+}]_e$ either alone (**gray**) or with the additional presence of TPEN (40 μM, 10 min before and during the OGD episode, **blue**) ($Ca^{2+}$ deregulation occurred after 11.5±0.4 min in 2 mM

$[Ca^{2+}]_e$, n=10; vs 19.4±1.26 min in 200 μM $[Ca^{2+}]_e$, n=7, $p<0.0001$ and after 27.4±0.47 min with TPEN in 200 μM $[Ca^{2+}]_e$, n=6, $p<0.002$, compared to low $Ca^{2+}$ alone).

**B:** In low (in 200 μM) $[Ca^{2+}]_e$, RR delays OGD evoked $Ca^{2+}$ deregulation. Slices were subjected to OGD alone or with RR (10 μM, 15 min prior, during and for 5 min after the OGD episode). Traces depict mean Fura-6F ratio changes (±SEM), and, as above, are aligned for onset of $Ca^{2+}$ deregulation (occurring after 19.4±1.26 min in control, **black**, n=7; vs 34.1±1.81 min with RR, **red**, n=6, $p<0.0001$).

**C:** In low (in 200 μM) $[Ca^{2+}]_e$, the selective MCU inhibitor, RU360 delays OGD evoked $Ca^{2+}$ deregulation. RU360 was pipette loaded into individual CA1 neurons (along with Fura-6F and FluoZin-3). Traces depict mean Fura-6F ratio changes (±SEM), and, as above, are aligned for onset of $Ca^{2+}$ deregulation (occurring after 19.4±1.26 min in control, **black**, n=7; vs 34.25±4.9 min, **red,** n=4, $p<0.01$).

**D:** RR exposure during OGD results in an accelerated intracellular $Zn^{2+}$ rise. Traces depict FluoZin-3 ($\Delta F/F_0$, **blue**) and Fura-6F ratio (**black**) changes in a single representative CA1 pyramidal neuron subjected to OGD in low $[Ca^{2+}]_e$ and the presence of RR. The arrow denotes the onset of the $Zn^{2+}$ rise. (The $Zn^{2+}$ rise occurred at 8.3±0.9 min, n=7 in control; vs 5.8±0.5 min, n=5 with RR, $p<0.05$, see **E**, below). After the sharp $Zn^{2+}$ rise, the progressive decrease in FluoZin-3 fluorescence is due to neuronal swelling that accompanies the ischemic insult, reflecting dilution of the indicator. The subsequent rise in $\Delta F/F_0$, at the time of RR washout reflects the fact that RR has a partial quenching effect on FluoZin-3 fluorescence, and the late decrease in fluorescence occurring at the time of $Ca^{2+}$ deregulation reflects a combination of highly accelerated swelling and loss of membrane integrity of the terminally injured cell, resulting in rapid dilution and loss of indicator. Notably, all of these effects seen with single wavelength indicators like FluoZin-3 are not seen with ratiometric indicators like Fura 6F, where the trace displays the ratio of emissions upon excitation at 340 and 380 nm that is substantially independent of dilution.

**E:** Effects of MCU blockers on the time of the $Zn^{2+}$ rise (**left**) and the time of the $Ca^{2+}$ deregulation (**right**). Bars depict mean values in minutes (±SEM).

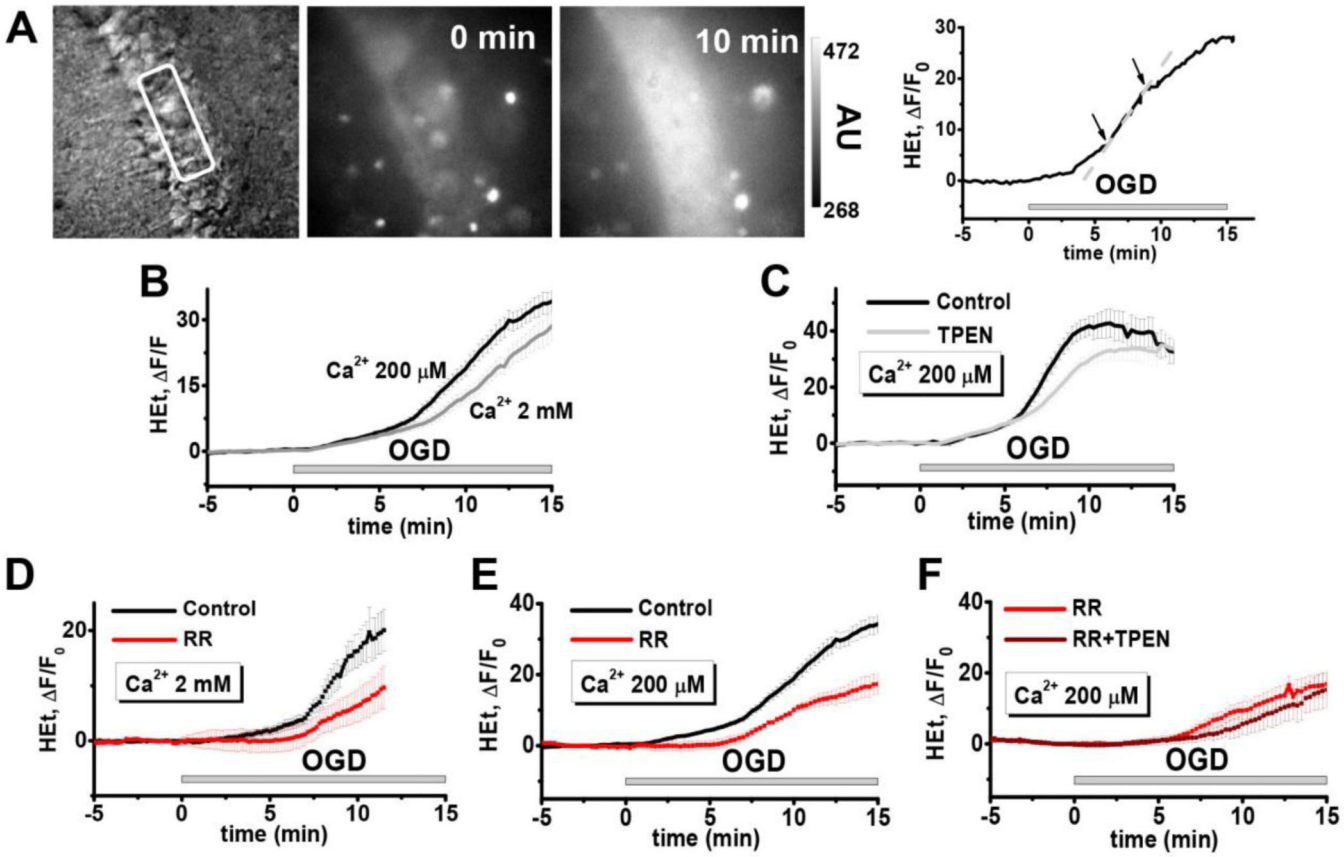


**Figure 3. OGD evokes ROS generation in CA1 pyramidal neurons**

Slices were bulk loaded with the superoxide preferring ROS indicator, hydroethidine (HEt, 20 μM for 30 min) and subjected to 15 min OGD.

**A:** OGD evokes HEt fluorescence increases (HEt ΔF) in CA1 neurons. A differential interference contrast image (**left**) shows the CA1 pyramidal cell layer from which HEt fluorescence changes were recorded; fluorescence images (**middle, right**) show representative HEt fluorescence before and after 10 min OGD as indicated. Trace (**far right**) shows HEt fluorescence changes (as $\Delta F/F_0$) in this slice in the region indicated by the rectangle. Arrows show approximate range of the steep phase of the HEt ΔF rise, used for linear fitting for slope determination (as described in methods); the dashed line shows a linear fit of this region.

**B**: Decreasing $[Ca^{2+}]_e$ accelerates OGD evoked ROS production. A set of matched slices was subjected to OGD. Graph represents mean HEt ΔF (±SEM) in the CA1 region of the hippocampus in slices subjected to OGD in 2 mM (**gray**, n=12 slices) or 200 μM $[Ca^{2+}]_e$ (**black**, n=13 slices). Slopes of the steep phases of the HEt ΔF rises were determined by linear fitting as described (see Methods; also **A**, above); based on this analysis, we found the mean slope (***m***) of the HEt ΔF to be increased in low $[Ca^{2+}]_e$ (from ***m*** = 3.22±0.34 in 2 mM $[Ca^{2+}]_e$, **gray**, n=12; to 4.26± 0.35, **black**, n=13 slices, in 200 μM $[Ca^{2+}]_e$; $p<0.05$).

**C:** $Zn^{2+}$ chelation slows ROS production during OGD carried out in low $[Ca^{2+}]_e$. Slices were subjected to OGD in 200 μM $[Ca^{2+}]_e$ alone, or with TPEN. The presence of TPEN

significantly slowed the HEt ΔF rise (from ***m*** = 9.82±0.82 in control, **black**, n=7; to 6.42±0.41 with TPEN, **gray**, n=8 slices, $p<0.005$).

**D:** In 2 mM $[Ca^{2+}]_e$, MCU inhibition slows HEt ΔF increase during OGD. Brain slices were subjected to OGD along (**black**, n=5 slices) or in the presence of RR (10 μM, 15 min before and during OGD, **red**, n=5 slices). Traces show mean OGD evoked HEt ΔF (±SEM) in the CA1 region. However, in this condition, the accelerated neuronal death with RR causes loss of indicator and prevents accurate quantification of the HEt ΔF slopes.

**E:** In low $[Ca^{2+}]_e$, OGD evoked ROS production is attenuated by MCU inhibition. Slices were subjected to OGD in 200 μM $[Ca^{2+}]_e$ alone, or with RR. The presence of RR markedly slowed the HEt ΔF rise (from ***m*** = 4.1± 0.5, **black**, n=8 in control to 1.96±0.33, **red**, n=6 slices with RR, $p<0.02$). Traces show mean OGD evoked HEt ΔF (±SEM) in the CA1 region.

**F:** Combined $Zn^{2+}$ chelation and MCU inhibition has no greater effect on ROS production during OGD, than MCU inhibition alone. Slices were subjected to OGD in 200 μM $[Ca^{2+}]_e$ with RR (**red, *m*** = 1.96±0.33, n=6 slices) or with both RR and TPEN (**brown, *m*** = 2.12±0.24, n=5 slices, $p>0.05$).